

HFDB-02 Test Summary

S. Feher, G. Ambrosio, N. Andreev, E. Barzi, P. Bauer, S. Bhashyam, R. Carcagno, D. Chichili, K. Ewald, L. Imbasciati, P. Limon, M. Lamm, I. Novitski, D. Orris, Y. Pischalnikov, C. Sylvester, M. Tartaglia, J. Tompkins, A.V. Zlobin

Content:

1. Introduction.....	2
2. Quench history.....	2
3. Ramp rate dependence.....	8
4. Temperature dependence.....	6
5. Heater studies.....	7
5.1 Strip heater studies.....	7
5.2 Spot heater studies.....	10
5.3 Temperature margin studies.....	13
6. Strain gauge measurements.....	15
7. AC loss measurements.....	19
8. RRR measurement.....	23
9. Splice resistance measurements.....	24

1. Introduction

HFDB02 was completed on April 1, 2002. The magnet was installed into the VMTF dewar and it was electrically checked by the end of April 8th, 2002. The VMTF dewar was filled with liquid helium on April 9th. First thermal cycle of the magnet has been completed on April 12th. The magnet was removed from the dewar and in order to improve quench performance several modifications were made in IB3. The magnet was installed into the VMTF dewar on May 6th and it was cold by the end of the day May 9th. The second thermal cycle test was finished on May 11th.

2. Quench History

After the cooldown the magnet current was ramped up to 7000A and down without observing a quench. The target current for the second high current ramp was 10000A. The first quench occurred at 9237 A. After a short magnet training the magnet reached its plateau around 12000 A. Most of the quenches were inside the Top half of the coil. This part of the coil was not heavily instrumented with voltage taps so we were not able to pinpoint the quench locations. After thermal cycling the magnet the quench behavior didn't change. The quenches still appear at the same region. We even cooled the magnet down to 2.15 K. We have seen a little quench current decrease instead of any increase but the quench locations didn't change.

The quench history plot is presented in Figure 1. and in Table 1. Table 1 also contains the locations of the quenches. Voltage traces of voltage segments for a typical quench are plotted in Figure 2.

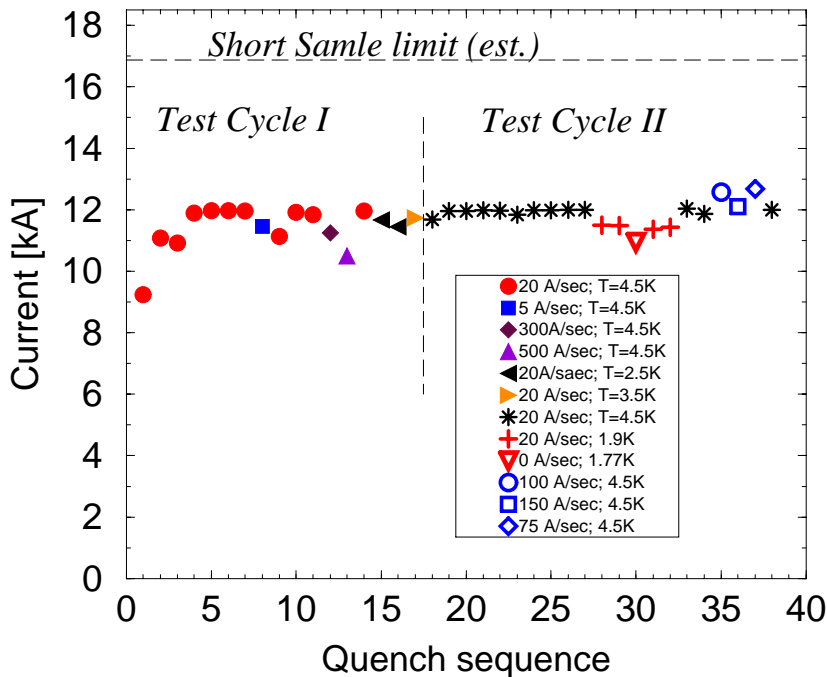


Figure 1. Quench history

Quench No.	File	Current	Temp. (K)	Ramp Rate	t_{quench}	MITs	Quench Start Voltage Tap Segment
1	hfdb02.Quench.020410140052.913	9237	4.5	20	-0.0122	3.45	BLRS2_QB1c
2	hfdb02.Quench.020410142750.904	11079	4.5	20	-0.0082	4.38	BLRS2_QB1c
3	hfdb02.Quench.020410151154.121	10914	4.5	20	-0.0038	3.76	T14c_QT2b
4	hfdb02.Quench.020410154240.292	11891	4.5	20	-0.0055	4.71	T14c_QT2b
5	hfdb02.Quench.020410161430.854	11967	4.5	20	-0.0058	4.75	T14c_QT2b
6	hfdb02.Quench.020410164840.126	11965	4.5	20	-0.0058	4.74	T14c_QT2b
7	hfdb02.Quench.020410172446.368	11959	4.5	20	-0.0078	5.05	T14c_QT2b
8	hfdb02.Quench.020410183140.141	11464	4.5	5	-0.0075	4.61	T14c_QT2b
9	hfdb02.Quench.020410190505.610	11124	4.5	20	-0.0219	6.17	T1c_QTLRS2
10	hfdb02.Quench.020410194959.169	11916	4.5	20	-0.0072	4.93	T14c_QT2b
11	hfdb02.Quench.020410202206.074	11834	4.5	20	-0.0088	5.08	T14c_QT2b
12	hfdb02.Quench.020410212535.348	11250	4.5	300	-0.0085	4.58	T14c_QT2b
13	hfdb02.Quench.020410215153.424	10496	4.5	500	-0.0098	4.15	T14c_QT2b
14	hfdb02.Quench.020411202227.581	11961	4.5	20	-0.0085	5.69	T14c_QT2b
15	hfdb02.Quench.020412095739.411	11674	2.45	20	-0.0101	5.42	T14c_QT2b
16	hfdb02.Quench.020412103324.584	11447	2.5	20	-0.0090	5.13	T14c_QT2b
17	hfdb02.Quench.020412122219.102	11738	3.5	20	-0.0070	5.01	T14c_QT2b
18	hfdb02.Quench.020509152319.016	11675	4.5	20	-0.0061	4.50	T14c_QT2b
19	hfdb02.Quench.020509155514.442	11957	4.5	20	-0.0063	4.72	T14c_QT2b
20	hfdb02.Quench.020509162505.294	11963	4.5	20	-0.0064	4.75	T14c_QT2b
21	hfdb02.Quench.020509165312.390	11978	4.5	20	-0.0076	4.91	T14c_QT2b
22	hfdb02.Quench.020509172013.590	11973	4.5	20	-0.0081	4.95	T14c_QT2b
23	hfdb02.Quench.020509175109.572	11837	4.5	20	-0.0078	6.05	T14c_QT2b
24	hfdb02.Quench.020509182344.478	11989	4.5	20	-0.0066	5.97	T14c_QT2b
25	hfdb02.Quench.020509190020.937	11989	4.5	20	-0.0060	5.85	T14c_QT2b
26	hfdb02.Quench.020509194825.491	11996	4.5	20	-0.0075	6.04	T14c_QT2b
27	hfdb02.Quench.020509203852.457	11998	4.5	20	-0.0079	6.14	T14c_QT2b
28	hfdb02.Quench.020511115520.123	11492	1.9	20	-0.0106	4.89	T14c_QT2b
29	hfdb02.Quench.020511123304.804	11488	1.9	20	-0.0109	4.91	T14c_QT2b

30	hfdb02.Quench.020511140911.348	10900	1.7	0	-0.0105	4.47	T14c QT2b
31	hfdb02.Quench.020511144347.511	11361	1.76	20	-0.0106	4.78	T14c QT2b
32	hfdb02.Quench.020511151901.432	11426	1.8	20	-0.0095	4.69	T14c QT2b
33	hfdb02.Quench.020511170643.980	12038	4.4	20	-0.0077	4.95	T14c QT2b
34	hfdb02.Quench.020511174223.729	11861	4.5	20	-0.0075	4.80	T14c QT2b
35	hfdb02.Quench.020511180539.327	12579	4.5	100	-0.0065	5.07	T14c QT2b
36	hfdb02.Quench.020511182952.865	12108	4.5	150	-0.0069	4.85	T14c QT2b
37	hfdb02.Quench.020511185201.536	12675	4.5	75	-0.0068	5.15	T14c QT2b
38	hfdb02.Quench.020511200428.870	12002	4.5	20	-0.0077	4.92	T14c QT2b

Table 1. Quench summary.

HFDB02 quench number 16

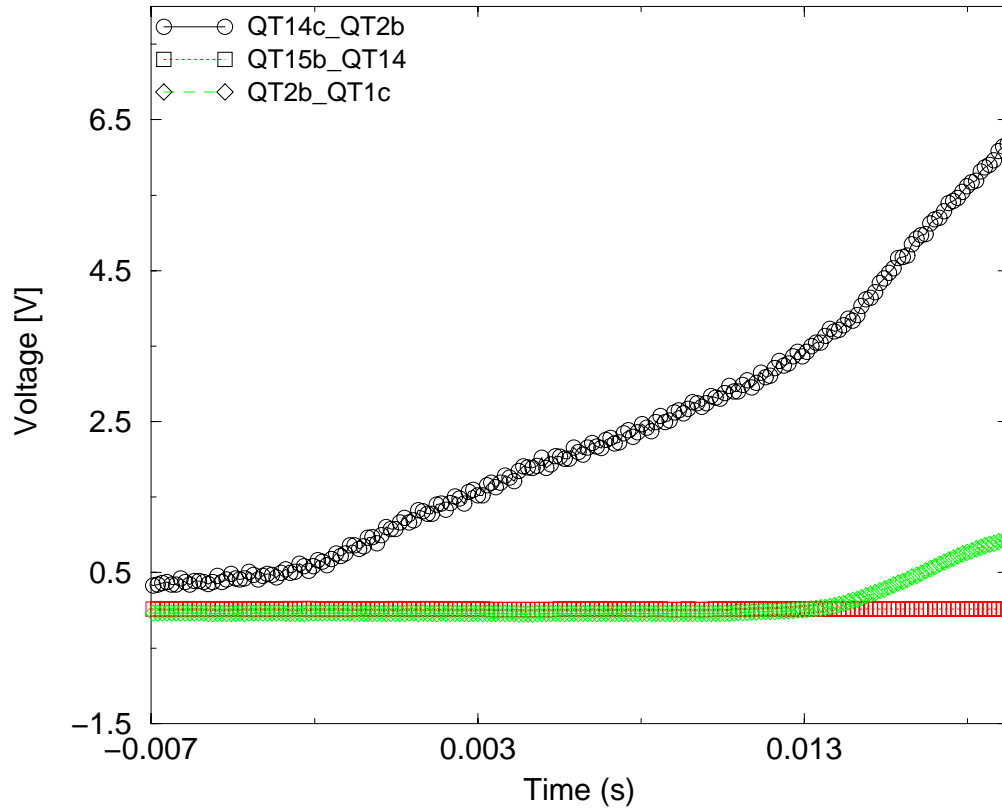


Figure 2. Quench number 16.

3. Ramp Rate Dependence

The default current ramp rate was 20 A/sec. The ramp rate dependence study is summarized in Figure 3. It was interesting that the ramp rate dependence showed a unique behavior: the quench current value had a maximum around 75 A/sec current ramp value.

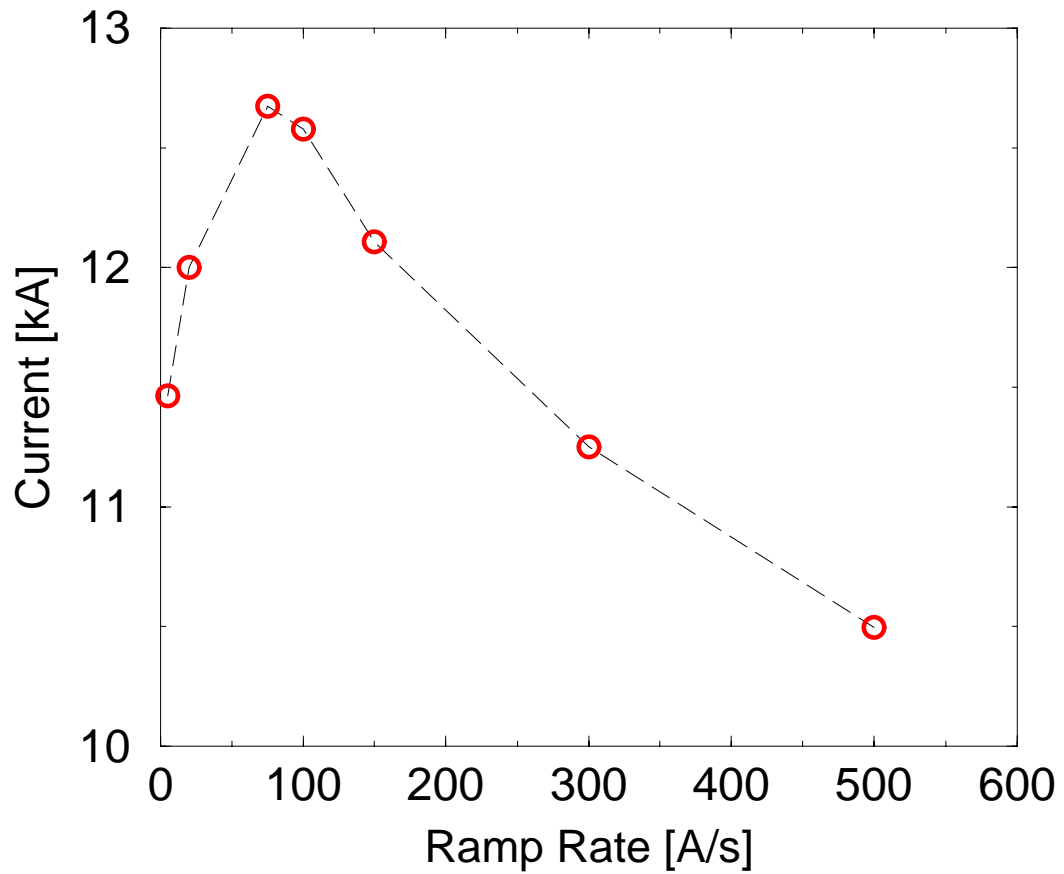


Figure 3. Current ramp rate dependence.

4. Temperature dependence

Temperature dependence plot is shown in Figure 4. It was remarkable that the quench current of this magnet exhibited opposite temperature dependence as one would expect. Decreasing the temperature of the bath, the quench current decreased as well.

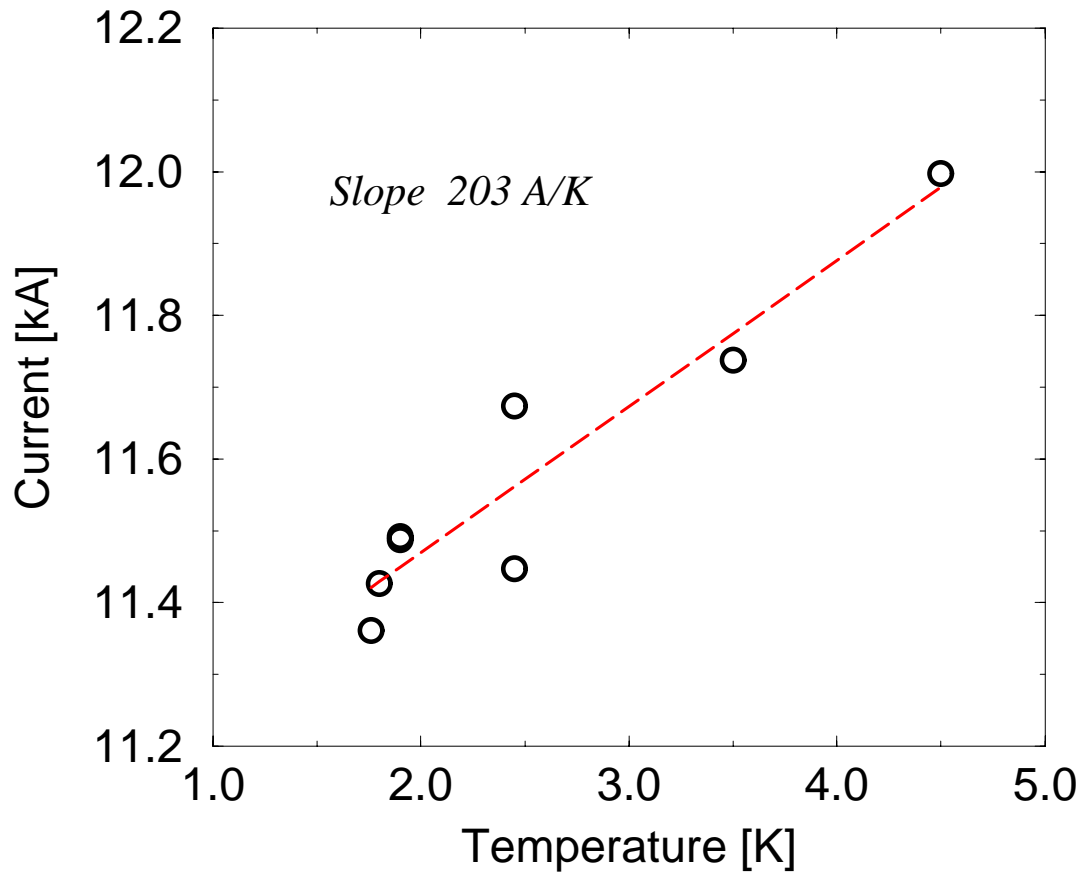


Figure 4. Temperature dependence.

5. Heater Study

5.1 Strip Heater studies

The quench heaters of HFDB02 consist of four SS strips: two strips for each coil, connected outside of the test facility. The quench heater for the bottom coil is placed on the inner side of the coil, close to the G10 middle plate. The heater is close therefore to the high field region. The quench heater for the top coil is placed on the outer side of the coil, close to SS external structure. Therefore, the heater is close to a low field region. On the other hand, when the magnet is exited, the Lorentz forces exert a pressure on the external heater that improves the thermal contact, and therefore the heater efficiency. This asymmetric position of the heaters allowed us to determine the outcome of the combined effect of magnetic field and pressure on the efficiency of the heaters, according to the different position. The heater studies were performed in the allowed current range, still far from the short sample limit. Different

electrical connection between the two heaters was used, starting from a series connection.

The collected data are presented in table 2 and in Figure 5-7.

	Current [A]	SHFU Voltage [V]	Tfn [sec]	Connections	Comment
1	3500	55	270	Series	Vmin
2	3500	75	140	Series	
3	3500	90	105	Series	
4	3500	100	90	Series	
5	7000	45	276	Series	Vmin
6	7000	55	145	Series	
7	7000	75	98	Series	
8	7000	100	73	Series	
9	10000	35	330	Series	Vmin
10	10000	50	110	Series	
11	10000	75	60	Series	
12	10000	100	54	Series	
13	10000	100	62	Parallel	
14	10000	200	39	Parallel	
15	3500	100	183	Parallel	
16	3500	200	68	Parallel	
17	10000	50	554	Top only	
18	10000	100	78	Top only	
19	10000	200	40	Top only	

Table 2: Heater study data

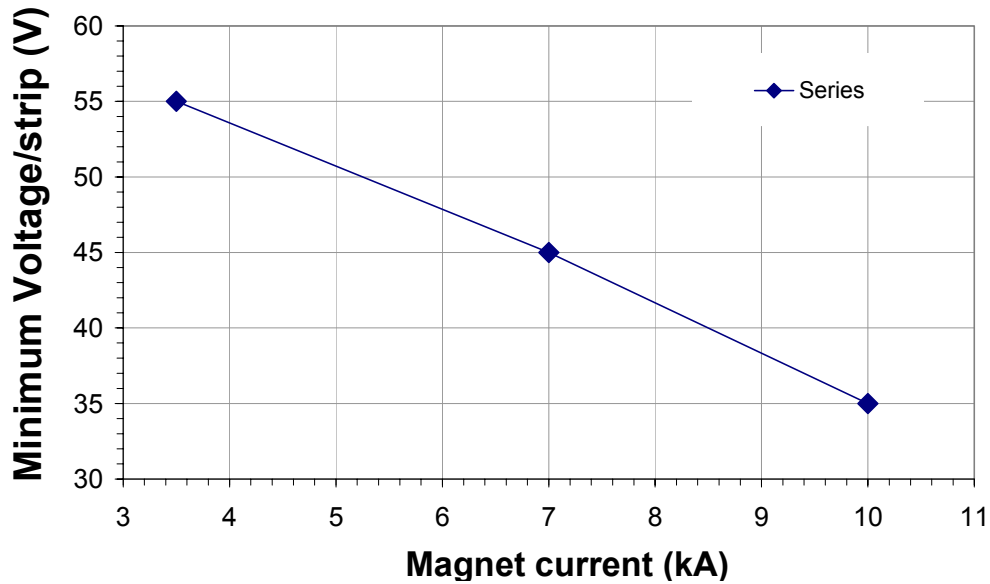


Figure 5. Minimum voltage study; the heaters were connected in series.

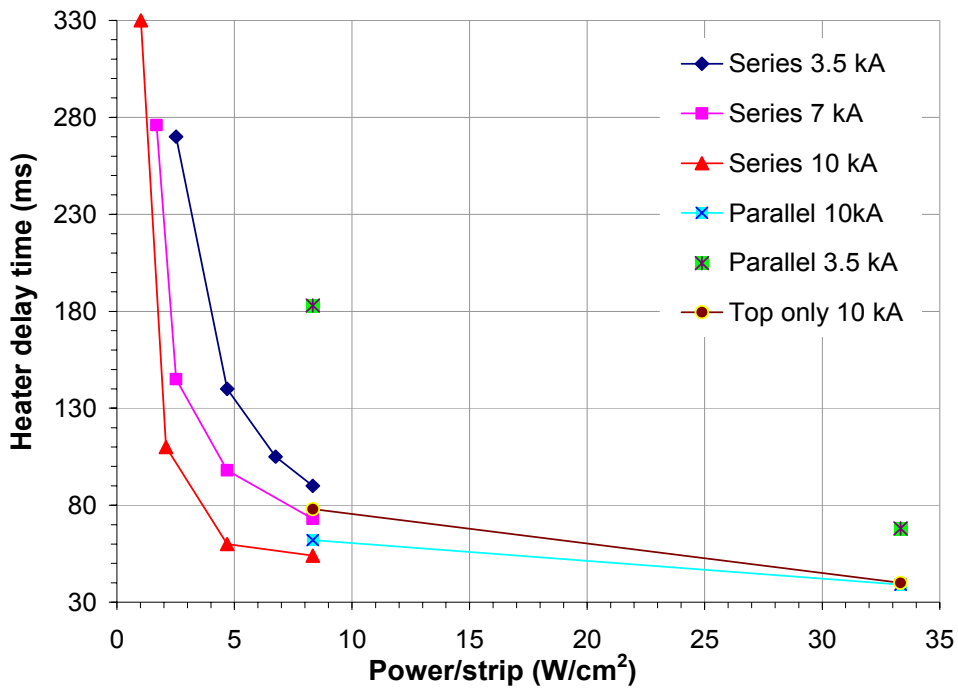


Figure 6. Time delay study

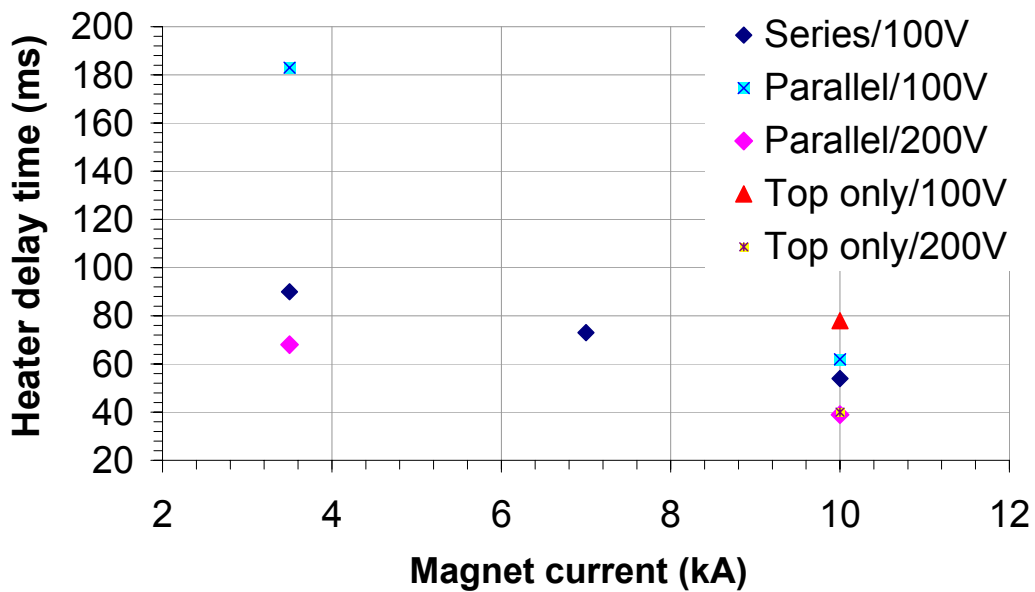


Figure 7. Time delay study

Summarizing the strip heater studies test results:

- The minimum delay time of about 40 ms was reached at 10 kA / $33 W/cm^2$, which was possible with the parallel connection and with the top heater only.
- With series and parallel connections, the quench started first in the bottom coil.

- With the top coil heater only, the heater delay time was ~20 ms more than with both active heaters, at the same power per strip, at low power.
- At high power per strip, the time delay was at the same level.

5.2 Spot Heater Study

HFDB02 was instrumented with two spot heaters, on the innermost turn of each coil, a temperature sensor close to each spot heater, and voltage taps across the spot heater regions. One voltage tap close to the spot heater of the top coil was damaged during fabrication (T28d2). Most of the studies were performed therefore on the bottom coil. Few test were performed also on the top coil and the results are similar.

Quench velocities studies were performed measuring the “time of flight”, that is the time difference between the quench signal of two voltage taps pairs. In Table 3, the voltage tap pairs, their distances and the velocity labels (used in Table 4 and Fig. 8) are indicated. The first two velocities are calculated over the distance from the spot heater center to the closest voltage taps, in the two directions (v_{0R} : towards return end; and v_{0L} : towards lead end). The last row is not related to the longitudinal quench velocity, but to the transverse quench propagation (turn-to turn), through the insulation. In table 4 all results are summarized.

Velocity Label	Voltage Tap # Pair 1	Voltage Tap # Pair 2	Distance (m)
v_{0R}	28d2-28d3	28d2-28d1	0.045
v_{0L}	28d2-28d3	28d3-28c	0.045
v_{1R}	28d2-28d1	28d1-28b	0.09
v_{1L}	28d3-28c	28c-28a	0.126
v_{2R}	28d1-28b	28d1-16b	0.325
t2t time	28d2-28d3	28d1-16b	Insulation

Table 3: Voltage taps schematic for quench velocity study.

Velocities (m/s)	Current	5 kA	7 kA	9 kA	10 kA	11 kA	11.5 kA
Thermal cycle 1	v_{0R}	1.2	2.6	4.5	4.5	7.5	
	v_{0L}	1	1.7	3.2	8.2	11.25	
	v_{1R}	2.5			7.4	8.2	
	v_{1L}	1.8					
	t2t (ms)	115			36	13	
Thermal cycle 2	v_{0R}	1.3	2.5	4.1	5.0		6.4
	v_{0L}	1.1	2.0	2.9	3.6		5.0
	v_{1R}	2.7	2.7	5.0	6.0		13
	v_{1L}	1.8					
	t2t (ms)	110			47		30

Table 4: spot heater test results: longitudinal quench velocity (m/s), and transverse propagation time (ms).

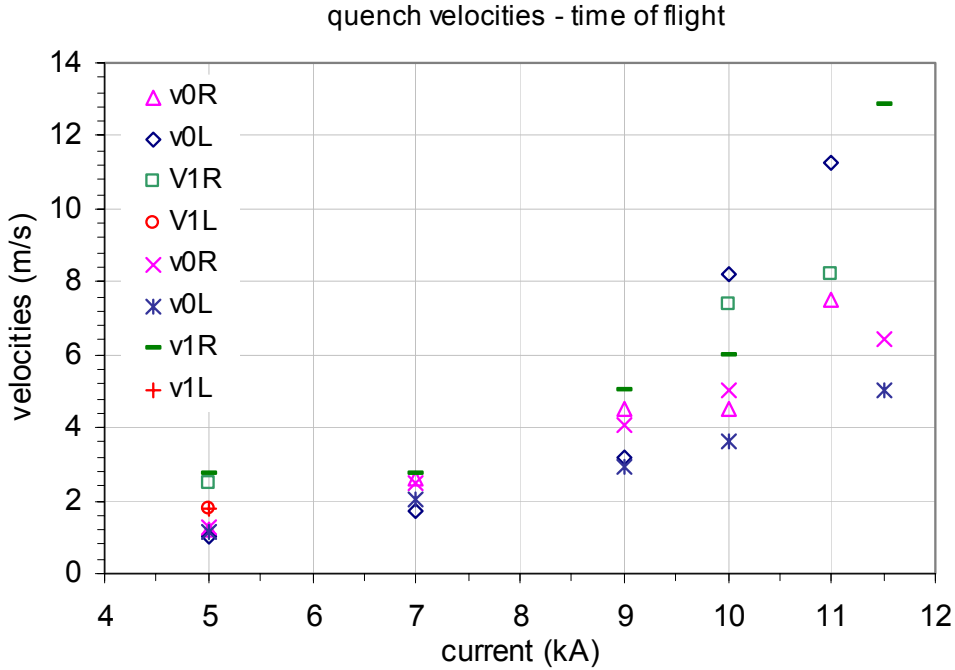


Figure 8. Longitudinal quench propagation velocities; closed symbols (as \square) refer to measurements taken during the first thermal cycle, and open symbols (as $+$) during the second thermal cycle.

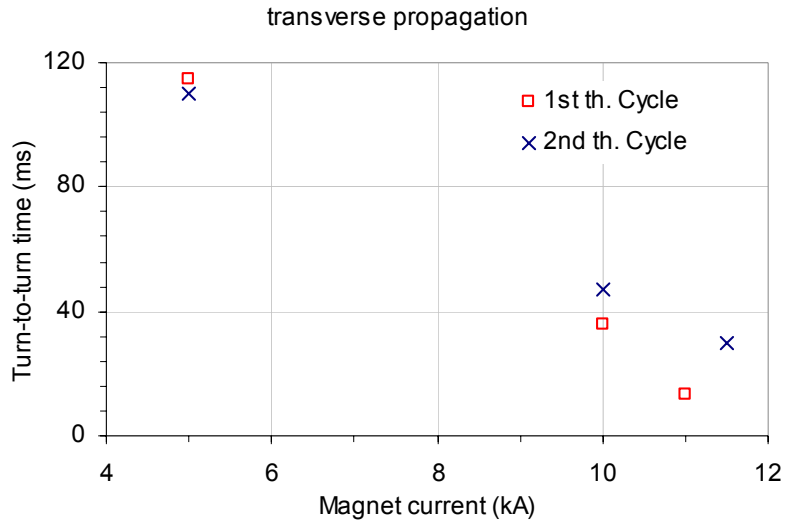


Figure 9. Transverse quench propagation times; close symbols refer to measurements taken during first thermal cycle, and open symbols during the second thermal cycle.

The velocities calculated with the time of flight are also consistent with the velocities calculated utilizing the slope of the resistance rise.

The precision of the data analysis was affected by the inductive noise that rises when the quench starts (Figure 10). In fact, the lost voltage tap in the top coil precluded the

possibility of reducing the noise by “buckling” the signal (that is subtracting the signal coming from voltage taps pairs in the same position in the two coils). This fact explains in part the large scattering of the results in Figure 8. Figures 10 and 11 show the voltage rise in case of, respectively, a spot-heater-induced quench (at 9925 A with voltage/length = 2 V/m), and a “spontaneous” quench (at 12675 A with voltage/length = 2.5 V/m). It is noticeable the much steeper voltage rise in case of the “spontaneous” quench.

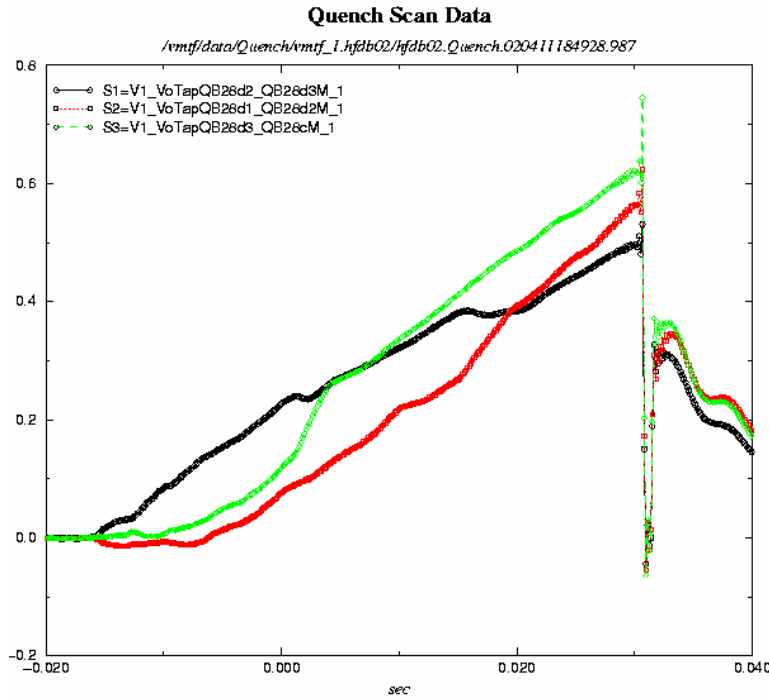


Figure 10. Voltage signals during a spot heater test.

Spot heater test:

- $dV/dt = 14 \text{ V/s}$;

Spontaneous quench:

- $dV/dt = 333 \text{ V/s}$, for the single turn signal (2b-1c, and 1c-lead);
- $dV/dt = 2*333 \text{ V/s}$, for the multi-turn signal (14c-2b).

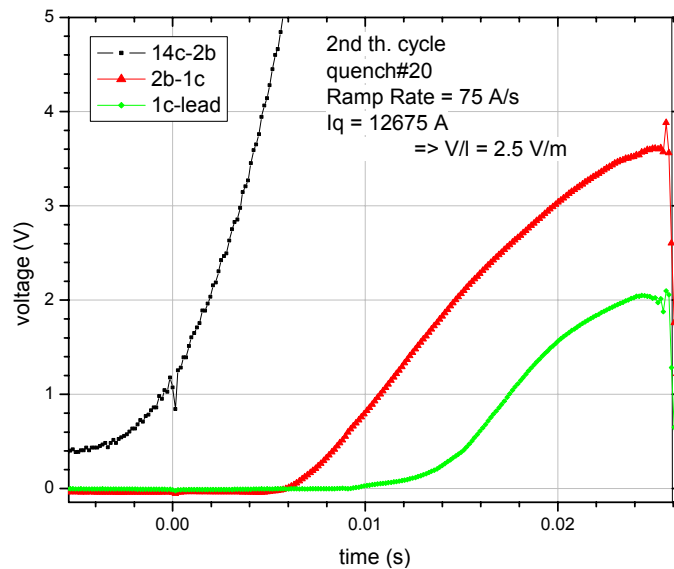


Figure 11. Voltage signals during a “spontaneous” quench.

5.3 Temperature margin measurements

These measurements are described in detail in TD-02-024. We report here briefly the procedure and the results.

The indirect critical current measurement consisted in operating the coils at a constant current, below the limiting current of ~ 12 kA. Subsequently the cable temperature was raised, sending a DC current through the 2.5 cm long spot heater (covering the cable over its entire width), while measuring the temperature rise in the cable a few mm up-stream with a calibrated Cernox sensor, until a quench occurred. The heater current was raised in small steps and the system was given time to establish equilibrium conditions after each step. The temperature at which a quench occurred in the cable (that is the current sharing temperature, referred to as “critical” temperature in the following for simplicity) can be, in conjunction with a critical surface parameterization, related to the cable critical current in the locations where the spot heaters and temperature sensors were located. The experimental results are shown in Figure 12.

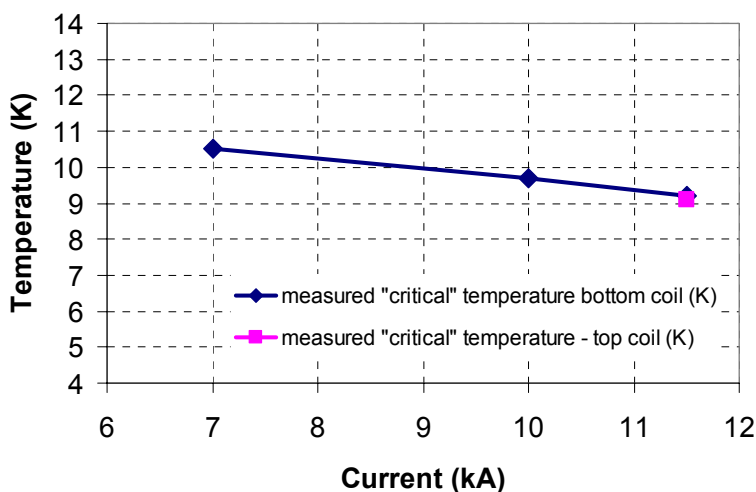


Figure 12: Temperature margin measurement, quench temperature versus magnet current; bottom and top coil – raw data.

Due to the fact that the temperature margin measurement was conducted in a 4.5 K background, temperature gradients are expected to occur at the edges of the zone heated by the 2.5 cm long spot heater. To calculate the temperature difference between the sensor and the cable at the hot spot, two ANSYS model were built.

The largest fraction of heat is exchanged into the direction perpendicular to the coils, through the main stainless steel plates. To quantify the heat flux into the different directions a 2D model of the racetrack magnet was built, which represents one quadrant of the cross section of the magnet. The x-axis runs along the width of the cable and the y-axis from cable to cable. The results of the model show that the heat flux through the thick stainless steel plates represents $\sim 80\%$ of the total flux, the rest remaining within the

coil plane. In fact, in the plane of the coils the heat is transported through the coils and G10 parts, which have lower heat conductivity.

A second 2D model represented the region close to the spot heater on the plane of a coil (x-axis along the cable and y-axis from cable to cable). The center-to-center distance between heater and temperature sensor is 16 mm. During the experiment, the current in the spot heater was increased up to ~ 0.5-0.6 A, generating therefore ($R_{heater}=2.3 \Omega$) a power of ~ 0.6-0.8 W. To take into account the heat conducted away in the other directions the second model was used, with a heater power which is only ~ 20 % of the actual, which corresponds to an input current ~ 40 % of the experimental heater current. The simulations were performed at different heater powers. The resulting maximum temperature in the cable close to the spot heater is a linear function of the temperature in the temperature sensor (averaged over the small area of the sensor), according to:

$$T_{cable} = 1.5 T_{sensor} (K) - 2.9 K .$$

Using this correction factor, the resulting temperature is in agreement with the critical temperature predicted by the critical current measurements of witness samples and taking into account the bending degradation due to React-and-Wind, as discussed in TD-02-024. Different models were used to predict the bending degradation, and the calculation of the critical surface at higher temperatures. The results are summarized in Figure 13.

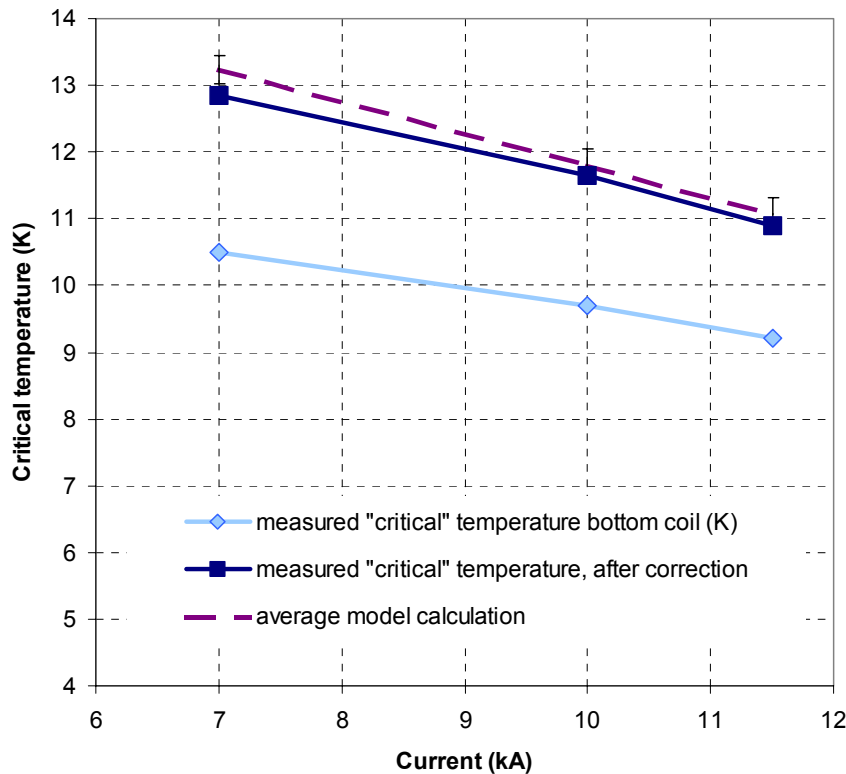


Figure 13: Comparison of temperature margin measurements and model predictions. The model predictions are represented by an “average” and “error” bars to show the variation.

6. Strain Gauge Studies

The strain gage data recorded during magnet excitation are presented in this section for both thermal cycle-I and thermal cycle-II. As noted in the production report (TD-02-032), four end bolts, four side bolts and four main bolts were instrumented with resistive strain gages. Two strain gages were mounted on each bolt and the readings from the two gages were averaged to eliminate any bending that may be occurring in the bolts. The instrumented end and main bolts were located close to the middle of the end and main plates, respectively, while the instrumented side bolts were located closer to the ends of the side plates. Some of the strain gages were lost between installation and final magnet excitation. All the instrumented main bolts showed the same behavior during magnet energization, as well as all the side bolts. On the contrary one end bolt showed a very different result from the others. In the following figures the bolt loads are presented for a typical main bolt, a typical side bolt, and two end bolts. Many quench tests were performed during both thermal cycles I and II, all strain gage data are reported for a typical case.

The strain gage data during magnet excitation for a typical main bolt(bolt #3) are presented in Figures 14 and 15 for thermal cycles I and II, respectively. Other bolts on the main plate demonstrated similar behavior for both cycles.

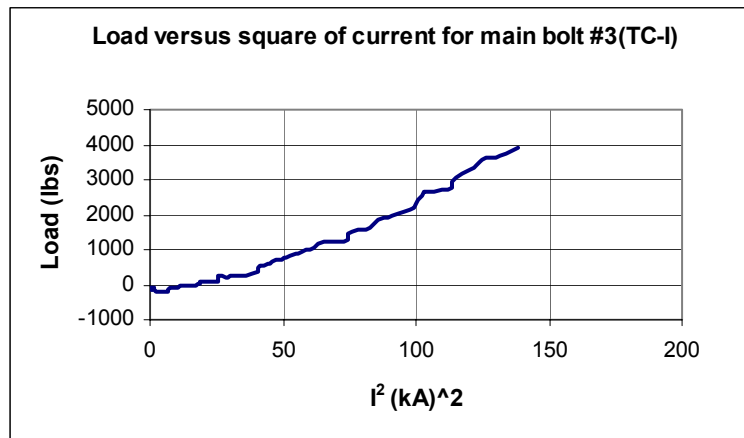


Fig 14. Main bolt loading during magnet excitation – TC-I

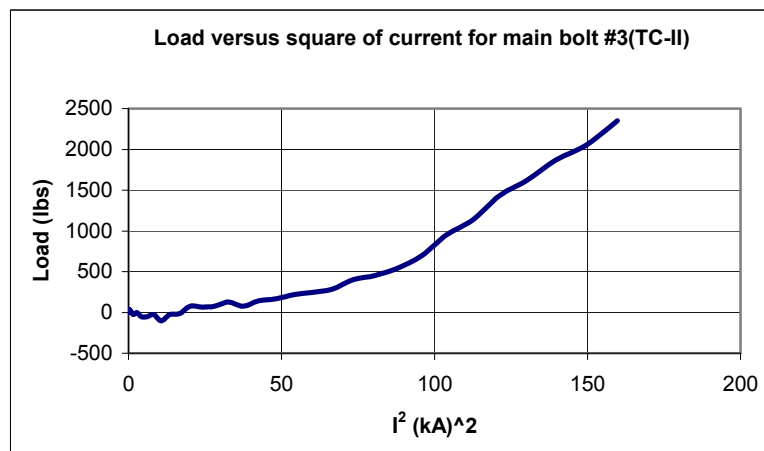


Fig. 15. Main bolt loading during magnet excitation – TC-II

The bolts demonstrate a more or less linear dependence on the square of the current in accordance with expected mechanical behavior.

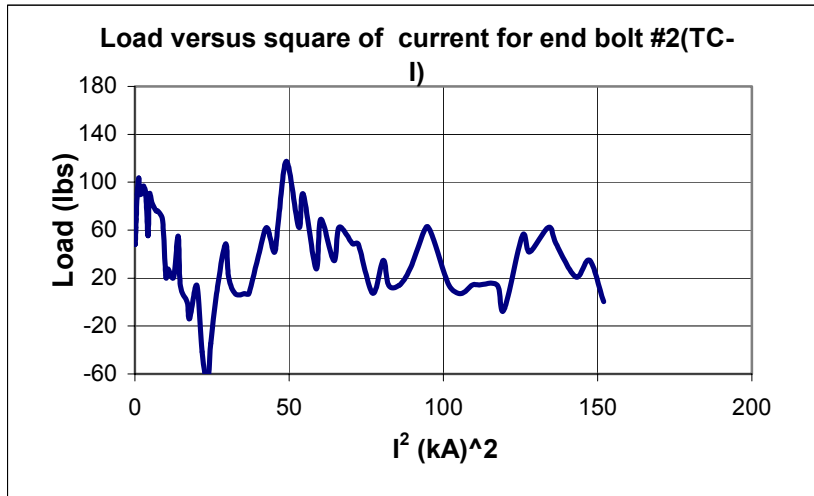


Fig. 16. End bolt loading during magnet excitation – TC-I

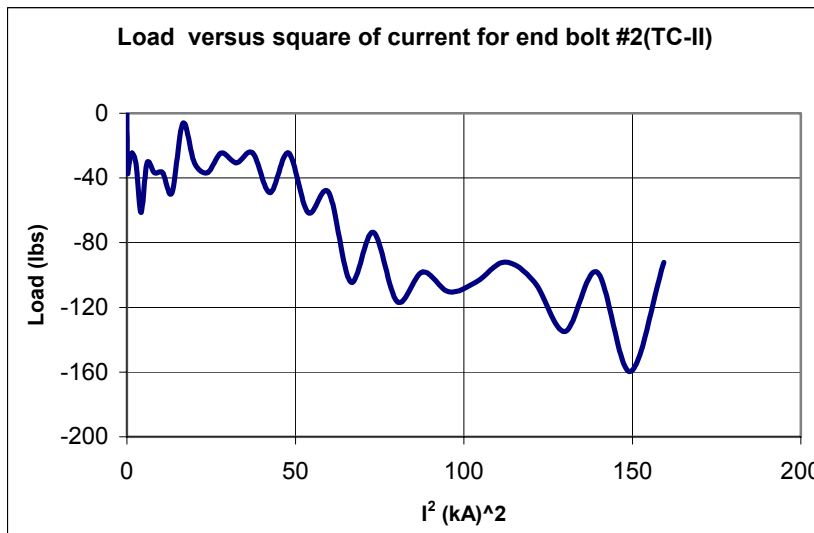


Fig. 17. End bolt loading during magnet excitation-TC-II

Figures 16 and 17 present typical end bolt loads for thermal cycles I and II, respectively. As can be seen from Figures 16 and 17, there is practically no loading on the end bolts during magnet excitation. The extent of variation of loads in Figures 16 and 17 is about the same level as noise present in the system. Other end bolts displayed similar behavior for both thermal cycles I and II. The only exception was that end bolt #4 (return end, bottom coil) showed a clear loading behavior during magnet excitation during thermal cycle II as shown in Figure 18.

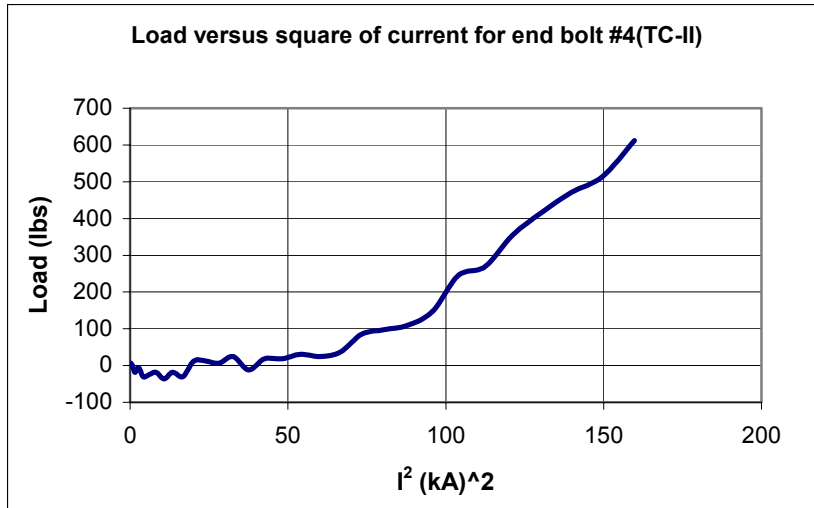


Fig. 18. End bolt loading (bolt #4) during magnet excitation –TC-II

Figure 19 and 20 present typical side loads during magnet excitation for thermal cycles I and II, respectively. As can be seen from figures 19 and 20, the side bolts exhibit a clear unloading behavior during magnet excitation. This was confirmed by comparing the raw resistances of the strain gages before excitation to resistance values during excitation. The resistance values of the gages during excitation were lower than the resistance values before excitation indicating unloading of the tensile pre-loads on the bolts. All other instrumented side bolts demonstrated similar behavior.

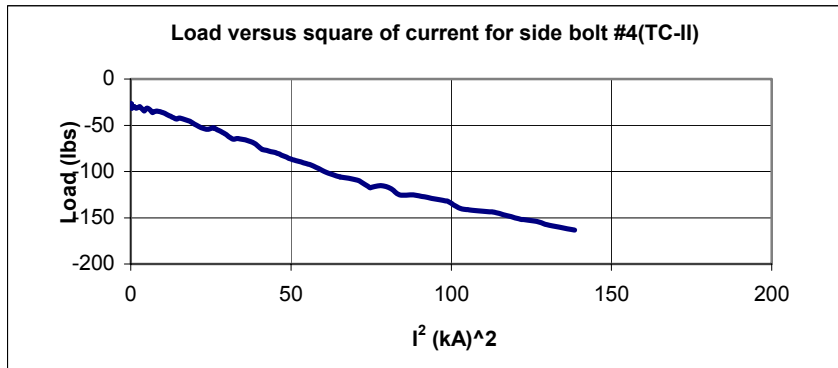


Fig. 19. Side bolt loading during magnet excitation – TC-I

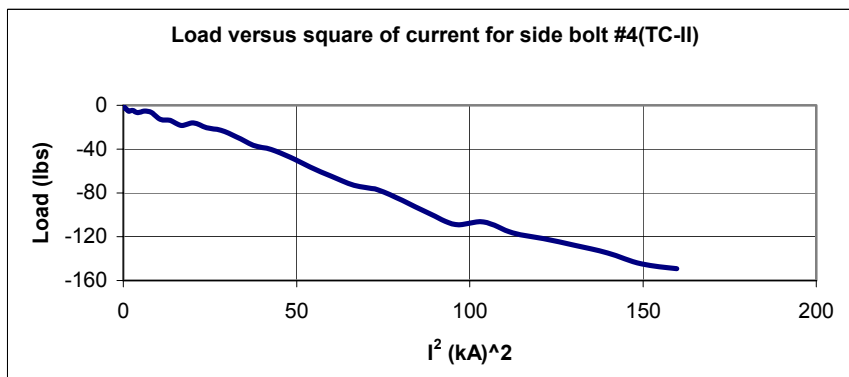


Fig. 20. Side bolt loading during magnet excitation – TC-II

Table 5 shows the load on the instrumented bolts during the second thermal cycle. The first column shows the pre-load measured immediately after pre-loading, the second column shows the pre-load measured at the test facility a couple of weeks later.

Bolt	300K IB3 after pre-stress (lbs)	300K VMTF (lbs)	4.2K VMTF after cool-down (lbs)	Cool-down Loss (lbs)	Energization Gain for 12 kA (lbs)
mainL1					
mainL2	2717	3445	4831	-1386	4600
mainR3	5973	5279	3146	2133	2350
mainR4	4058	5583	3465	2118	1290
AVG	4805	4769	3814	955	2747
lend1	3065	3264	2372	892	0
lend2	2870	2090	1005	1085	0
rend3	3001	3383			0
rend4	3664	3885	3445	440	600
AVG	3364	3156	2274	806	150
sideL1	2640	2605	2758	-153	-124
sideL2	2097	2037	1843	194	-130
sideR3	2078	2209	2116	93	-171
sideR4	2287	2282	2466	-184	-150
AVG	2276	2283	2296	-13	-144

Lost strain gages

Table 5: Summary of bolt data during the second thermal cycle.

7. AC loss measurements

Energy Loss measurements were performed on HFDB02 at 4.5K using two HP3458A Digital Multimeters (dmm) setup to integrate over 1 power line cycle and sample at 60Hz. One dmm measured the magnet voltage and the second dmm measured the magnet current via a 20KA Holec Transductor. The magnet was ramped between 500A and 6500A for all measurements. Five measurements were performed at each ramp rate of 75A/s, 100A/s, 150A/s, 200A/s, 250A/s, 300A/s, and 400A/s, and three pre-ramp cycles were performed before each new ramp rate.

The measured **Hysteresis = 347 Joules**
And the measured **Slope = -0.05 J/A/s**

The following is a plot of the data (see next page):

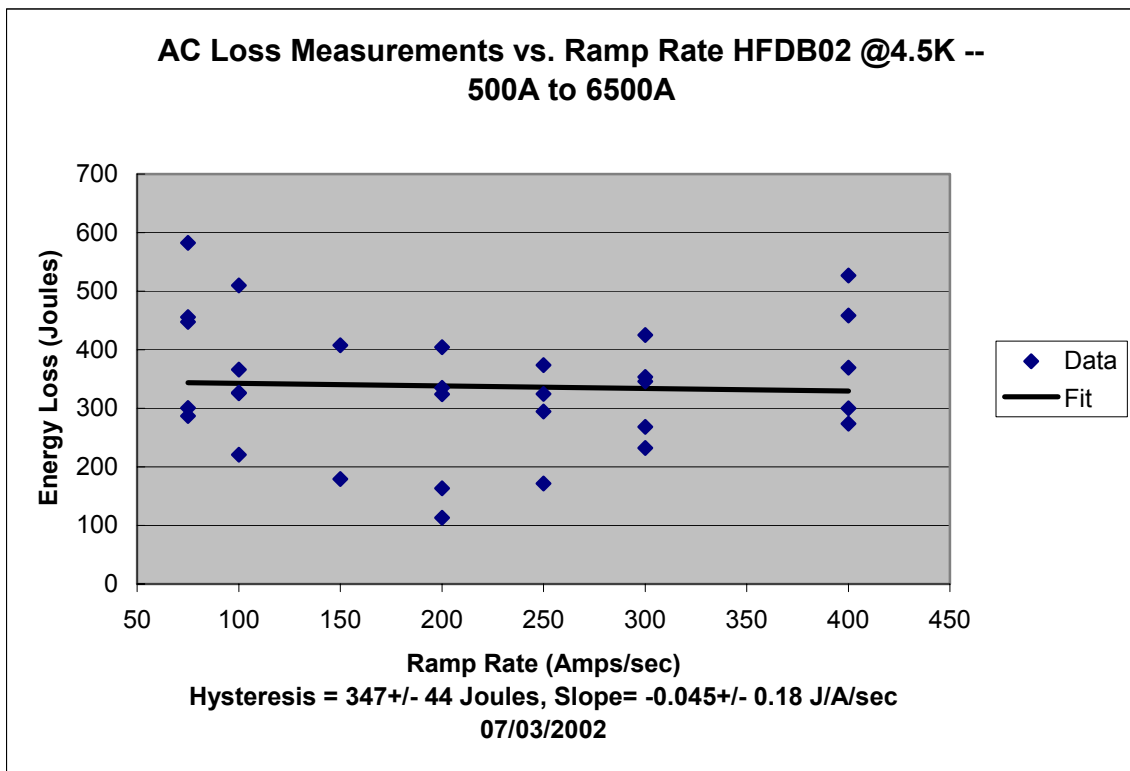


Figure 21. AC loss measurement plot as a function of current ramp rate.

<i>Ramp Rate(Amps/sec)</i>	<i>Energy Loss(Joules)</i>	<i>Integral Volts</i>
75	456	0.0134
75	301	-0.0144
75	448	-0.0039
75	582	0.0387
75	287	-0.0221
100	327	-0.0154
100	510	0.0261
100	366	0.0001
100	221	-0.0322
100	325	-0.0063
150	407	-0.0001
150	179	-0.0406
200	404	0.0119
200	113	-0.0468
200	335	-0.0121
200	163	-0.0249
200	324	-0.0189
250	172	-0.0352
250	374	-0.0019
250	295	-0.0045
250	325	-0.0170
300	425	0.0032
300	346	-0.0076
300	268	-0.0129
300	354	-0.0079
300	232	-0.0153
400	369	-0.0010
400	527	0.0346
400	274	-0.0149
400	458	0.0208
400	300	-0.0096

Table 6: Energy Loss Measurement @ 4.5 K; cycle: 500 – 6500 – 500 A

Power Loss was determined from the frequency of the ramp, which was calculated based on the measured end points of the ramp.

The measured **Slope = 362 Watt/Hz**
And the measured **Intercept = 0.36 Watts**

The following is a plot of the data (see next page):

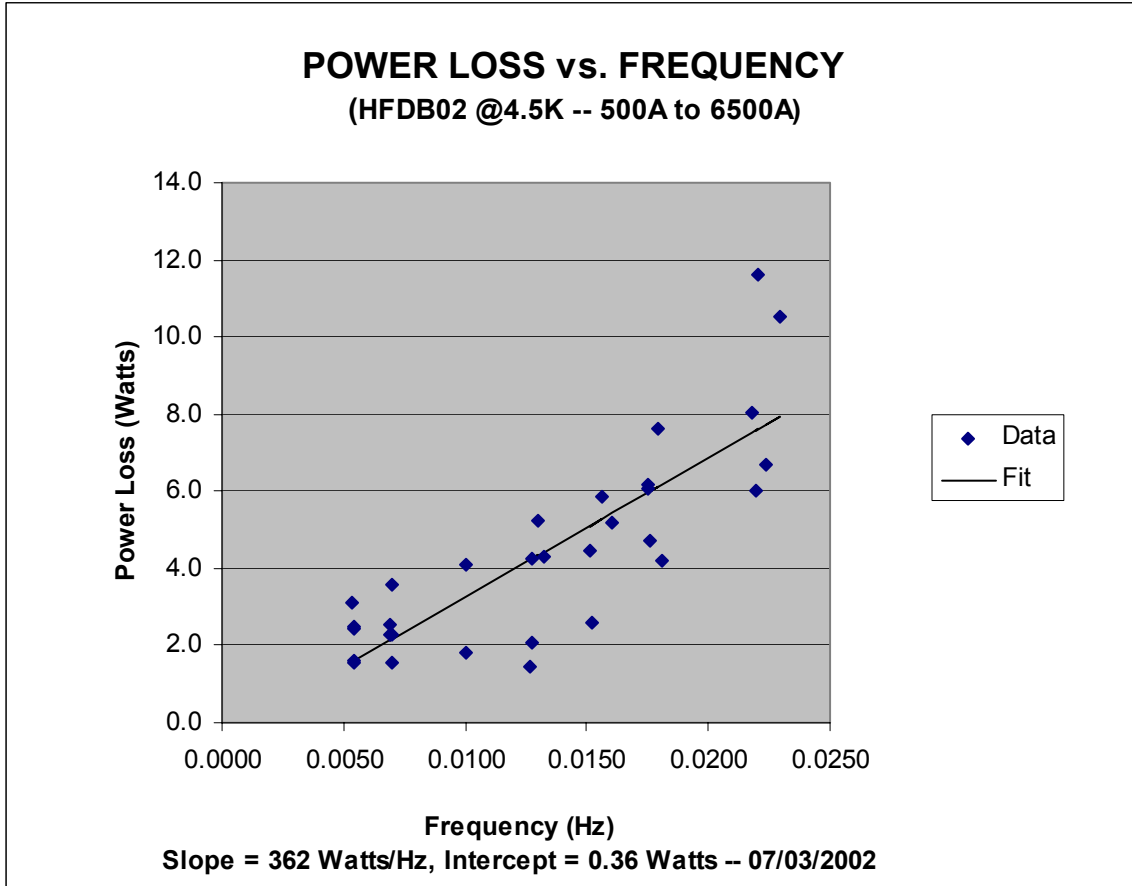


Figure 22 Power loss measurement plot as a function of frequency.

Ramp Rate (A/sec)	Frequency (Hz)	Power Loss (W)
75	0.0055	2.5
75	0.0054	1.6
75	0.0054	2.4
75	0.0053	3.1
75	0.0054	1.6
100	0.0070	2.3
100	0.0070	3.6
100	0.0069	2.5
100	0.0070	1.6
100	0.0069	2.3
150	0.0101	4.1
150	0.0100	1.8
200	0.0130	5.3
200	0.0127	1.4
200	0.0127	4.3
200	0.0127	2.1
200	0.0132	4.3
250	0.0152	2.6
250	0.0157	5.9
250	0.0151	4.5
250	0.0160	5.2
300	0.0179	7.6
300	0.0175	6.1
300	0.0176	4.7
300	0.0175	6.2
300	0.0181	4.2
400	0.0218	8.0
400	0.0221	11.6
400	0.0220	6.0
400	0.0230	10.5
400	0.0224	6.7

Table 7: Power Loss Measurement @ 4.5 K; cycle: 500 – 6500 – 500 A

8. RRR measurement

The RRR measurement was performed on 4/15. While the racetrack coil was gradually warming up, we recorded the whole coil voltage value generated by ± 10 A across the magnet. The low temperature plot and the corresponding magnet voltage is shown in Figure 23 and 24. The measured RRR value is 23.

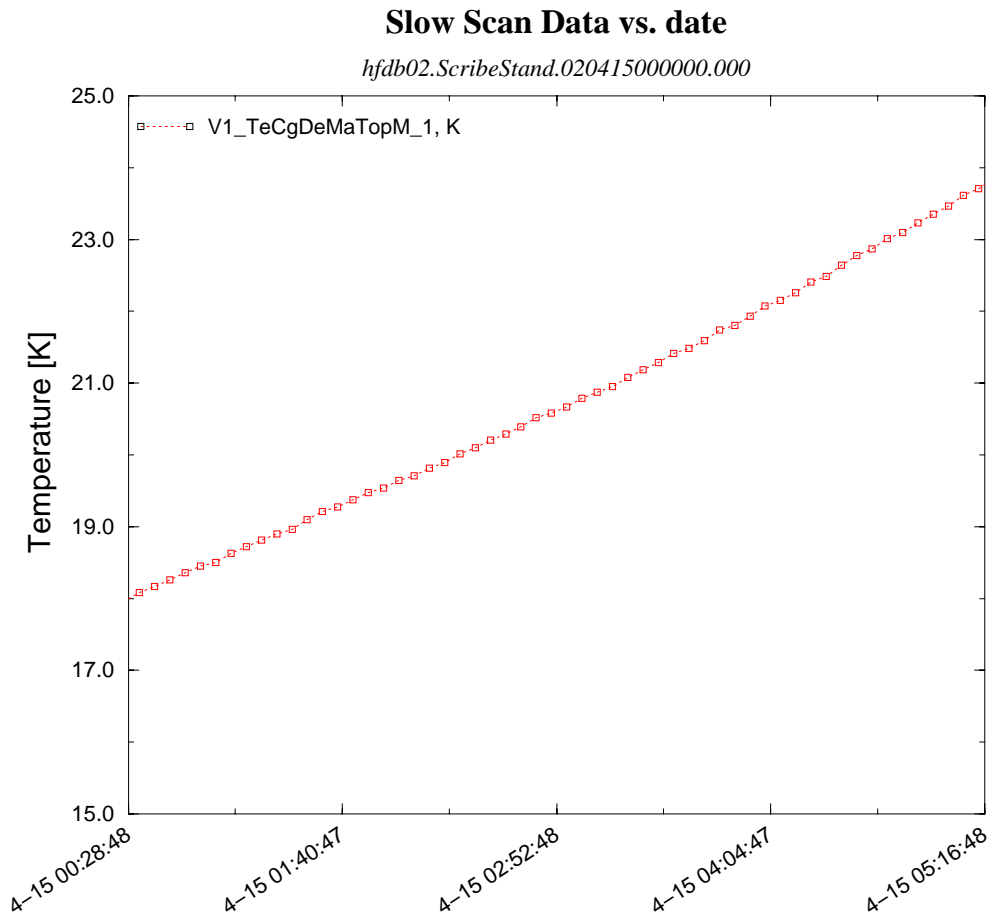


Figure 23. Temperature plot as a function of time.

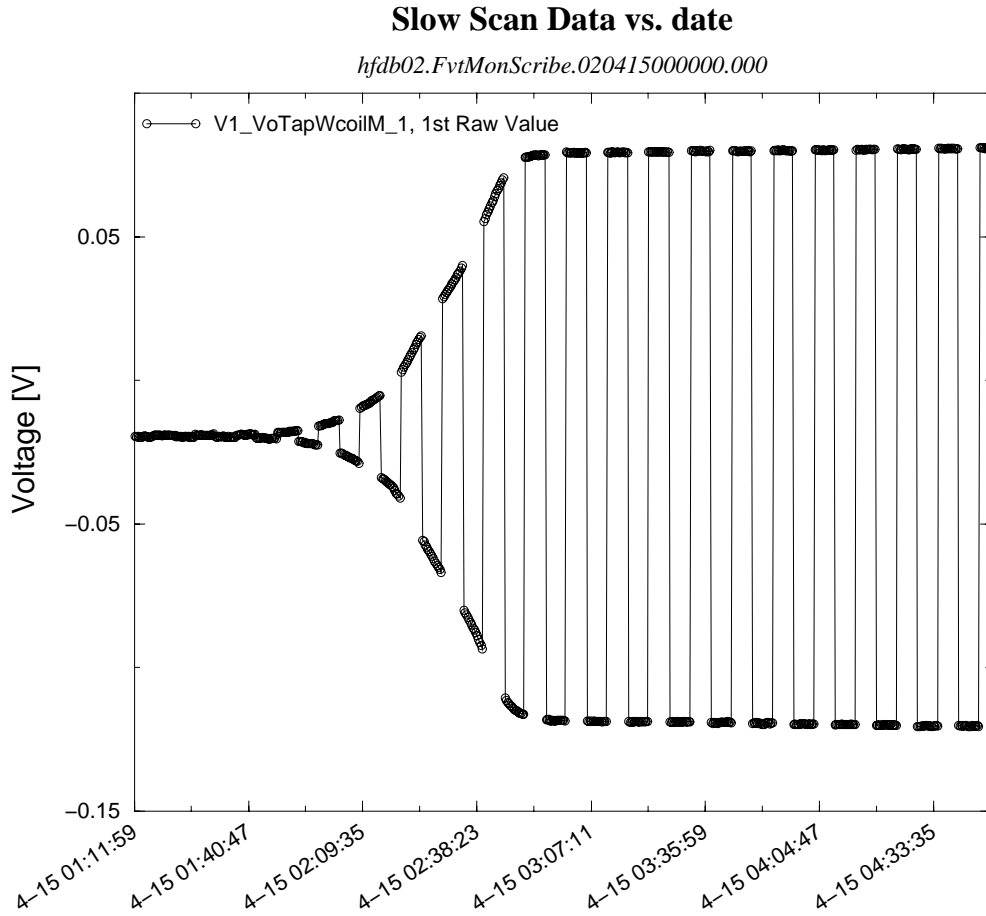


Figure 24. Whole coil voltage plot as a function of time.

9. Splice resistance measurement

The resistance of the splices (two at the leads and two inner splices) was measured at 6 and 11 kA. The measurements were very noisy and many data were taken at each current in order to reduce the noise.

	Bottom Lead	Top Lead	Bottom Inner	Top Inner
	nΩ	nΩ	nΩ	nΩ
@ 6 kA	1	0.8	2.3	2.2
@ 11 kA	0.8	0.7	2.2	2.3

Table 8: Splice resistance.